Controlling a Spillover Pathway with the Molecular Cork Effect

Matthew D. Marcinkowski[1], April D. Jewell[1], Michail Stamatakis[2], Matthew B. Boucher[3], Emily A. Lewis[1], Colin J. Murphy[1], Georgios Kyriakou[1] & E. Charles H. Sykes[1*]

[1]*Department of Chemistry, Tufts University, Medford, MA 02155-5813*
[2]*Department of Chemical Engineering University College London, Torrington Place, London WC1E 7JE, United Kingdom*
[3]*Department of Chemical and Biological Engineering, Tufts University, Medford MA 02155-5813*
* charles.sykes@tufts.edu

Spillover of reactants from one active site to another is important in heterogeneous catalysis and has recently been shown to enhance hydrogen storage in a variety of materials[1–7]. The spillover of hydrogen is notoriously hard to detect or control[1,2,4–6]. We report herein that the hydrogen spillover pathway on a Pd/Cu alloy can be controlled by reversible adsorption of a spectator molecule. Pd atoms in the Cu surface serve as hydrogen dissociation sites from which H atoms can spillover onto surrounding Cu regions. Selective adsorption of CO at these atomic Pd sites is shown to either prevent the uptake of hydrogen on, or inhibit its desorption from, the surface. In this way, the hydrogen coverage on the whole surface can be controlled by molecular adsorption at a minority site, which we term a "molecular cork" effect. We show that the molecular cork effect is present during a surface catalyzed hydrogenation reaction and illustrate how it can be used as a method for controlling uptake and release of hydrogen in a model storage system[1,2,4–6,8].

Hydrogen activation, uptake, and reaction are important phenomena in heterogeneous catalysis, fuel cells, hydrogen storage devices, materials processing and sensing[1–11]. Much attention has been devoted to materials that exhibit facile activation and weak binding of hydrogen, as these properties lead to the best energy landscape for storage or chemical reactivity[12–14]. Spillover is a common method by which a reagent can be activated at one location and then reacted at another, and it is commonly invoked to explain the synergistic relationship between metals in an alloy or metal/metal oxide mixtures[1,3–7,12,15]. For example, in heterogeneous catalysis hydrogen spillover from metal particles to reducible oxide supports is implicated as an important step in a variety of reactions including hydrogenations, hydroisomerizations, and methanol synthesis[1,3,6]. Hydrogen spillover has also been shown to significantly enhance the performance of hydrogen storage materials such as metal organic frameworks, zeolites and many carbon-based nanostructures[2,4–6]. In these cases, the addition of small metal particles, typically Pt or Pd, promotes uptake by activating molecular H_2 and facilitating spillover of hydrogen atoms (H_a) onto the support. Despite these advances, the mechanism of spillover in most systems remains poorly understood, and with the exception of hydrogen bridges[16] in storage systems, methods for mediating the spillover pathway do not exist. In this paper we describe how the hydrogen spillover pathway on the Pd/Cu alloy system can be controlled via the reversible adsorption of a spectator molecule (CO) at minority Pd atom sites. The use of a model system amenable to study by scanning tunnelling microscopy (STM) was critical in order to monitor the detailed

distribution of Pd atoms, H_a and CO molecules, all of which are distributed heterogeneously at the atomic-scale. This information can then be related to temperature programmed desorption/reaction (TPD/R) data, and complex phenomena like spillover, competitive adsorption and storage can be understood[12,17–20].

It is well established that at low coverages (typically less than 0.1 monolayers (ML)), Pd atoms in the surface of Cu(111) exist predominantly as individual atoms that are isolated from one another[20–23]. For this reason we term this particular type of alloy a *single atom alloy* (SAA)[12]. Fig. 1a shows the atomic-scale structure of such a SAA surface formed by depositing 0.01 ML of Pd on Cu(111) at a surface temperature of 380 K. This large scale image reveals that the Pd/Cu alloy is formed at the ascending step edges, leading to a rumpled appearance in the STM image termed a "brim". As the distance from the step edge increases, the amount of Pd decreases to the point where little Pd is present on much of the Cu terrace. The high resolution inset shows atomic resolution of the brim in which the Pd atoms appear ~20 pm higher than the surrounding Cu atoms and illustrates that they are spatially isolated from one another. We have previously demonstrated that such Pd/Cu SAA surfaces are active for H_2 dissociation[12,20]. Fig. 1b depicts H_a on a Cu terrace that originated from the dissociative adsorption of 2 L (L, 10^{-6} torr·s) of H_2 at Pd sites followed by spillover of H_a onto the Cu surface. Due to their lower density of states near the Fermi level, adsorbed hydrogen atoms appear as ~10 pm depressions in STM images[12]. TPD measurements reveal that in the reverse process, H_2 is released from this surface in a single state centred at 210 K. A representative TPD spectrum is shown in Fig. 2a that resulted from a 200 L dose of hydrogen on the 1% Pd/Cu alloy surface at 85 K, corresponding to a H_a coverage of 0.2 ML. The desorption mechanism is depicted in the schematic of Fig. 2a. Individual Pd atoms bind H slightly more strongly, but offer a much lower barrier for dissociation and recombination as compared with Cu[20]. Therefore, as the system is heated the lowest energy pathway for hydrogen to escape the surface is via a Pd atom, as dictated by microscopic reversibility[24]. In this way the minority 1% Pd atoms act as a low energy entrance and exit routes for hydrogen to adsorb and desorb from the Cu surface. The overall behaviour also suggests that the availability and residence of H_a on the Cu surface may be finely tuned by adjusting the state of these Pd sites. For example, by utilizing a spectator molecule that preferentially occupies the Pd brim, the Pd sites can be selectively blocked.

In this regard, CO is an excellent candidate molecule as it adsorbs reversibly on both Cu and Pd surfaces and interacts much more strongly with low index Pd surfaces (500 K desorption) as compared to Cu (170 K desorption)[25–27]. The STM image shown in Fig. 1c was obtained after exposing the 0.01 ML Pd/Cu SAA surface to a small amount (0.03 L = 0.003 ML) of CO at 5 K followed by annealing the sample to 60 K. Fig. 1c reveals that the adsorbed CO molecules also appear in STM images as depressions with an apparent depth of ~15 pm. Depositing a very small amount of CO and subsequently annealing the sample below CO's desorption temperature resulted in the migration of the CO exclusively to the 1% atomic Pd sites in the brim (upper right side of image) indicating that at equilibrium Pd sites are preferred. To support this conclusion we performed molecular manipulation experiments in which, using voltage pulses (4.8 V) delivered by the STM tip, CO molecules were desorbed one-by-one. We then interrogated the nature of the surface sites beneath with atomic resolution. Figure 1d-f shows an example in which an individual CO molecule was removed from its preferred adsorption site prior to the area being completely cleared of CO and imaged

with atomic resolution (see Supplementary Fig. S1 for the complete experimental sequence). These experiments reveal an exact correlation between CO adsorption site and individual Pd atoms in the surface beneath and show that one CO molecule is adsorbed above each Pd atom in the surface. When the Cu/Pd SAA surface was exposed to 0.01 ML of CO at 150 K followed by 200 L of H_2 at 85 K, the only desorption product observed was CO, in a peak centred at 270 K (Fig. 2b). CO desorption at 270 K is intermediate between desorption from Cu(111) and Pd(111), consistent with CO adsorbed at atomic Pd sites[25–27]. Note that the small exposure of CO ensures that the Pd brim is occupied by CO while the Cu terraces remain essentially CO free. Our quantitative TPD experiments allow us to titrate just enough CO to cover the 1% Pd sites but leave the Cu surface bare as shown in Supplementary Figs. S2 and S3. The absence of H_2 desorption indicates that, despite the availability of clean Cu sites for accommodating H_a, the Pd sites are blocked by CO molecules, which inhibit the dissociation of H_2 and the spillover of H_a. Similar active site blocking/poisoning effects for surface step edges have been reported in the literature[17–19]. When the order of CO and H_2 exposures was reversed, such that 200 L of H_2 followed by 0.01 ML of CO were deposited, a more significant effect occurs. As shown in Fig. 2c, the H_2 desorption peak is observed but is shifted 50 K higher in temperature to 260 K and is 20 K narrower than in the absence of CO.

This result indicates that CO adsorption at the minority 1% Pd sites blocks the re-association and desorption of H_2 at 210 K, the temperature at which H_2 would normally desorb. The inset of the spectrum in Fig. 2c reveals that the desorption of H_2 begins as soon as the first CO desorbs. Moreover, the desorption of H_2 also occurs over a smaller temperature range as H_a is trapped on the surface above its normal desorption temperature in a higher energy state. These points will be discussed in detail in terms of our simulations. The schematics in Fig. 2 illustrate this new phenomenon that we term a "molecular cork" effect. H_a spills onto the Cu terraces filling the "bottle" via a Pd atom "bottleneck". The bottle is then "corked" by adsorption of CO, preventing hydrogen from leaving until it is "uncorked" by CO desorption. If the cork is put in place prior to H_2 exposure, it is impossible for H_2 to get through the bottleneck, and no uptake is observed. In this way uptake on the whole surface can be turned on and off by the molecular cork at a minority (1%) site, and most importantly, hydrogen can be trapped on the surface above its normal desorption temperature. Corking and poisoning are not the same; poisoning is a stoichiometric effect in which the active sites of a catalyst are blocked one by one, whereas in the cork effect, blocking a minority site affects the reactant coverage of the whole surface. We show that the cork effect enables control of a catalytically important spillover pathway between two metals by selective molecular adsorption at atomic sites[17–19]. CO adsorption enables hydrogen to be stored on the surface beyond its normal desorption temperature as shown in the isothermal experiments in Supplementary Fig. S4.

In terms of the interaction of CO with Pd/Cu alloy sites, both experimental and density functional theory (DFT) work indicate that CO interacts strongly with Pd atoms in the surface layer of bimetallic Pd/Cu systems[25–28]. The trend in the adsorption states/energies as a function of Pd concentration predicts that CO binds preferentially to higher coordinated Pd sites i.e. sites with more than one Pd atom. If the concentration of Pd is very small, as in our system, the CO is predicted to bind to sites atop the individual Pd atoms[26–28]. This is consistent with one CO molecule being adsorbed at each Pd atom as confirmed by our STM molecular manipulation experiments. We

hypothesize that the binding of CO to Pd in these SAAs electronically alters the Pd atoms, thus increasing the dissociation/recombination barrier and forcing H_a to adsorb/desorb only in the absence of CO[26–28].

To support the experimental observations, we modelled the system using the kinetic Monte Carlo (KMC) method (see Supplementary Figs. S5-7). The simulations of the TPD spectra shown in Fig. 3 are in excellent agreement with experiments, and are able to capture both the shift of the H_2 peak centre to higher temperatures as well as the narrower peak width in the corked system (Figs. 3A and B). In an ensemble of 25 such KMC simulations, the average desorption temperature for the uncorked system was calculated to be ~211 K and a similar simulation scheme for the corked system yielded an average H_2 peak temperature of 246 K.

The H_a and CO coverages on the Pd/Cu surface were also investigated to further elucidate the microscopic details of the spillover and desorption pathways. In both systems the hydrogen coverage on the Pd/Cu sites remained high even when the coverage on the Cu sites dropped significantly due to the stronger binding of hydrogen on the former. Thus, at the initial stages of H_2 desorption, H_a diffused from the Cu sites to the Pd/Cu sites where it rapidly recombined and desorbed, only in the absence of CO. As H_a was depleted, the coverages on the two site types dropped while remaining in quasi-equilibrium (see also Supplementary Fig. S6). In all simulations, H_2 was observed to desorb from Pd/Cu sites and only when the adjacent Pd site was no longer occupied by CO (for a statistical analysis of the events simulated refer to Supplementary Fig. S7), indicating that the adsorption/desorption processes were microscopically reversible. On average (from 25 simulations), 119 H_2 molecules exited the surface via a single Pd atom site after just one CO molecule desorbed. This theoretical result supports our experimental observation that H_2 begins to desorb as soon as the first CO desorbs as seen in Fig. 2c and is in complete agreement with the conceptual model of the molecular cork presented in Fig. 2. Experiments performed at faster heating rates lead to higher temperature desorption of hydrogen as would be expected for a process dictated by desorption of CO. Molecular corking, as the term implies, is therefore a kinetic effect by which hydrogen is trapped in a non-equilibrium state.

This molecular cork effect is not limited to CO, as we also observe it during a surface-catalyzed chemical reaction in the absence of CO. We have recently shown that the Pd/Cu SAA is capable of hydrogenating styrene to ethylbenzene[12]. When 0.01 ML of Pd was added to a Cu(111) surface and exposed to 400 L of H_2 at 85 K in the absence of CO, H_2 desorbed in a single state centred at 205 K as shown in Fig. 4. Exposing the same surface to 400 L of H_2 at 85 K followed by 0.06 ML of styrene (1) at 150 K yields the selective hydrogenation to ethylbenzene (2), during which the H_2 peak is shifted higher in temperature to 260 K. The inset of Fig. 4 shows the desorption profiles of the hydrogenation product ethylbenzene and some un-reacted styrene. These results reveal that the presence of the reactants and products of a chemical reaction can themselves cork the atomic Pd sites in the same way as CO. Even a small amount of styrene (0.01 ML) corks a 1% Pd/Cu alloy surface (See Supplementary Fig. S8). Interestingly, as the cork effect produces trapped H_a, it may serve to increase the product yield in the hydrogenation reaction by keeping H_a on the surface at higher temperatures and allowing further hydrogenation to occur than if the reaction terminated at 205 K when the H_2 left the surface. A modest shift of ~50 K in the H_2 desorption temperature is predicted to have a large effect on conversion to products given that the rates of activated reactions increase rapidly with temperature. However, it is not possible to

compare the reactivity of "uncorked" and "corked" H_a because the reactants themselves act as a cork.

While we have used a model system to illustrate the molecular cork effect in hydrogen dissociation and spillover between different regions of a Pd/Cu surface, we expect that this effect should be somewhat general for any heterogeneous system with a similar energetic landscape. Species other than CO should act as molecular corks and allow spillover between sites to be controlled. Many promising hydrogen storage materials require extremes of pressure or temperature to charge/discharge efficiently[2,4–6,16], and unwanted hydrogen release at ambient temperatures is often a problem[2]. We suggest that rather than altering the storage material or the pressure of the container vessel, a chemical approach involving treatment with small amounts of a molecular cork molecule could be used to retard hydrogen desorption and enable long-term storage under ambient conditions. This is a reasonable proposal given that many systems that operate via spillover from small metal particles exhibit lower uptake/release barriers, reversible adsorption/desorption isotherms and even memory of sequential doses of H_2 and D_2 isotopes during discharge[5,16]. In terms of catalysis, while weak binding is desirable for efficient, low temperature operation, processes with higher barriers to reaction cannot proceed as hydrogen is not stable on the surface at higher temperatures[13]. The molecular cork effect serves to retain weakly bound, trapped H_a on the surface at higher temperature in a potentially more reactive form[29]. Given that the rates of chemical reactions increase rapidly with temperature, trapping H_a on the surface ~50 K beyond its desorption temperature should have a significant impact on conversion to products. This approach opens up interesting possibilities to activate reactions with higher barriers utilizing this new non-equilibrium state of surface-bound hydrogen.

In summary, we show that the spillover process, and hence the coverage of the entire surface, can be controlled via molecular adsorption at minority (1%) sites in a reversible manner. This is very different to the traditional picture of most interfacial processes, which involve uniform adsorption, reaction, and desorption of molecules. We show that CO adsorption can be used to block the hydrogen desorption channel, leading to a buildup of 2D pressure and the eventual fast release of the hydrogen at higher temperatures: a phenomenon we term the "molecular cork" effect. This non-equilibrium process produces trapped, higher energy hydrogen atoms, which are potentially more reactive than regular surface bound hydrogen. We also suggest that the molecular cork effect could offer a new method for mediating the kinetics of hydrogen uptake and release from storage materials that rely on spillover from small metal particles.

Methods
Experimental

Two ultra-high vacuum (UHV) instruments were used to perform the experiments, both of which have been described in detail elsewhere[12]. Briefly, the first UHV system was operated at a base pressure of <1 x 10^{-10} mbar and contains a quadrupole mass spectrometer used for temperature programmed desorption/reaction (TPD/R) measurements and has facilities for Auger electron spectroscopy (AES) and low energy electron diffraction (LEED). Hydrogen 99.999% (AirGas) was deposited on to the sample by means of a 6 mm diameter collimator tube pointed directly at the sample. Hydrogen coverage calculations were based on a saturation coverage of unity when hydrogen was adsorbed on a 4 monolayer (ML) Pd film, assuming that the film

terminates as Pd(111). CO and styrene coverages refer to saturation of their respective monolayer TPD peaks[12]. Carbon monoxide 99.99% (AirGas) and high purity styrene 99.9% (Aldrich) were deposited on the sample by backfilling the chamber to the required pressure. Styrene was purified on receipt by many freeze-pump-thaw cycles. Styrene yields were recorded with a heating ramp of 1 Ks^{-1} by tracking the parent ion m/z 104. Ethylbenzene yields were recorded by tracking the parent ion at m/z 106 as well as the fragment at m/z 91. The presence of styrene fragments in the desorption profile of ethylbenzene can be subtracted in order to produce the desorption profile of ethylbenzene. In the present set of TPR measurements, a very low coverage of styrene was utilized (0.06 ML), which made a negligible contribution to the ethylbenzene desorption profile; therefore, spectra subtraction was not performed. The spectrum obtained from m/z 91 is the one shown for ethylbenzene.

The second chamber was an Omicron Nanotechnology LT-UHV STM used for high-resolution imaging of the alloy samples. The base pressure in the low-temperature chamber was <5 x 10^{-11} mbar. The instrument incorporated a preparation chamber in which cleaning, annealing and Pd deposition were performed. CO and hydrogen dosing in the LT-STM was performed through a line-of-sight doser aimed directly at the Cu(111) sample in the STM stage. The STM stage was held at either 80 K or 5 K during dosing, and could be cooled from 80 K to 5 K after dosing for imaging of hydrogen. Pd deposition was performed in both UHV systems using flux monitored Omicron Nanotechnology Focus EFM 3 electron beam evaporators. The Cu(111) samples were held at 380 K during deposition. Pd coverages were calibrated using both AES and TPD of CO.

Theoretical

For the kinetic simulations, an in-house FORTRAN code implementing the graph-theoretical KMC simulation method[30] was used. The code input consists of a lattice structure, the binding configurations of the species (along with the corresponding energies), an initial lattice configuration, the reaction mechanism and the simulation conditions. Lattice structure: the Pd/Cu(111) catalytic surface was represented as a triangular lattice with 2163 atop Cu and 237 atop Pd sites. The latter were randomly placed under the restriction that they cannot be neighbours. The three-fold Cu and Pd/Cu sites were also explicitly taken into account. Binding configurations: the simulation accounts for two binding configurations for H adatoms (on the three-fold Cu and Pd/Cu sites) and one for CO molecules (on the atop Pd sites). The binding energies were taken from previous literature and adjusted to match the experiments. Initial configuration: 1600 H adatoms were distributed among the three-fold Cu and Pd/Cu sites according to Fermi-Dirac statistics at the initial simulation temperature. For the corked system, 237 CO molecules were placed on atop Pd sites covering all such sites. Reaction mechanism: seven reversible elementary processes were taken into account, in particular, (i) CO adsorption/desorption on atop Pd sites; H_2 dissociative adsorption/aissociative desorption on three-fold Cu sites (ii), on three-fold Pd/Cu sites in the absence of CO (iii) and in the presence thereof (iv), as well as H adatom diffusion between three-fold Cu sites (v), from three-fold Cu to a three-fold Pd/Cu sites (vi), and between three-fold Pd/Cu sites (vii). For each reaction, forward and backward elementary steps were considered (for instance adsorption/desorption), and all reaction energies were calculated from the binding energy data for each species to ensure

thermodynamic consistency. Kinetic parameters were evaluated using literature data and adjusted to match the experiments. Hydrogen diffusion was treated as a fast quasi-equilibrated process. <u>Simulation conditions</u>: the initial temperature was 160 K and a temperature ramp of 1.0 K/s was used. Zero partial pressures were assumed for both H_2 and CO in the gas phase. More information on the simulation setup and the calculation of kinetic parameters is presented in section KMC Methodology Details of the Supplementary Information.

References

1.   Conner, W. C. & Falconer, J. L. Spillover in heterogenous catalysis. *Chem. Rev.* 95, 759–788 (1995).
2.   Graetz, J. New approaches to hydrogen storage. *Chem. Soc. Rev.* 38, 73–82 (2009).
3.   Jung, K.-D. & Bell, A. T. Role of hydrogen spillover in methanol synthesis over Cu/ZrO_2. *J. Catal.* 193, 207–223 (2000).
4.   Cheng, H., Chen, L., Cooper, A. C., Sha, X. & Pez, G. P. Hydrogen spillover in the context of hydrogen storage using solid-state materials. *Energy Environ. Sci.* 1, 338–354 (2008).
5.   Wang, L. & Yang, R. T. Hydrogen storage on carbon-based adsorbents and storage at ambient temperature by hydrogen spillover. *Catal. Rev. Sci. Eng.* 52, 411–461 (2010).
6.   Prins, R. Hydrogen spillover. facts and fiction. *Chem. Rev.* 112, 2714–2738 (2012).
7.   Merte, L. R. *et al.* Water-mediated proton hopping on an iron oxide surface. *Science* 336, 889–893 (2012).
8.   Groß, A. Hydrogen on metal surfaces: forever young. *Surf. Sci.* 606, 690–691 (2012).
9.   Wei, J., Ji, H., Guo, W., Nevidomskyy, A. H. & Natelson, D. Hydrogen stabilization of metallic vanadium dioxide in single-crystal nanobeams. *Nat. Nanotechnol.* 7, 357–362 (2012).
10.   Eliaz, N., Eliezer, D. & Olson, D. L. Hydrogen-assisted processing of materials. *Mater. Sci. Eng., A* 289, 41–53 (2000).
11.   Shegai, T., Johansson, P., Langhammer, C. & Käll, M. Directional scattering and hydrogen sensing by bimetallic Pd-Au nanoantennas. *Nano Lett.* 12, 2464–2469 (2012).
12.   Kyriakou, G. *et al.* Isolated metal atom geometries as a strategy for selective heterogenous hydrogenations. *Science* 335, 1209–1212 (2012).
13.   Greeley, J. & Mavrikakis, M. Alloy catalysts designed from first principles. *Nat. Mater.* 3, 810–815 (2004).
14.   Chopra, I. S., Chaudhuri, S., Veyan, J. F. & Chabal, Y. J. Turning aluminium into a noble-metal-like catalyst for low-temperature activation of molecular hydrogen. *Nat. Mater.* 10, 884–889 (2011).
15.   Wittstock, A., Zielasek, V., Biener, J., Friend, C. M. & Bäumer, M. Nanoporous gold catalysts for selective gas-phase oxidative coupling of methanol at low temperature. *Science* 327, 319–322 (2010).
16.   Li, Y. & Yang, R. T. Hydrogen storage in metal-organic frameworks by bridged hydrogen spillover. *J. Am. Chem. Soc.* 128, 8136–81377 (2006).
17.   Hahn, C., Shan, J., Groot, I. M. N., Kleyn, A. W. & Juurlink, L. B. F. Selective poisoning of active sites for D_2 dissociation on platinum. *Catal. Today* 154, 85–91 (2010).
18.   Vang, R. T. *et al.* Controlling the catalytic bond-breaking selectivity of Ni surfaces by step blocking. *Nat. Mater.* 4, 160–162 (2005).
19.   Gambardella, P. *et al.* Oxygen Dissociation at Pt Steps. *Phys. Rev. Lett.* 87, 0561031–0561034 (2001).
20.   Tierney, H. L., Baber, A. E., Kitchin, J. R. & Sykes, E. C. H. Hydrogen dissociation and spillover on individual isolated palladium atoms. *Phys. Rev. Lett.* 103, 2461021–2461024 (2009).

21. Bellisario, D. O. *et al.* Importance of kinetics in surface alloying: a comparison of the diffusion pathways of Pd and Ag atoms on Cu(111). *J. Phys. Chem. C* 113, 12863–12869 (2009).

22. Tierney, H. L., Baber, A. E. & Sykes, E. C. H. Atomic-scale imaging and electronic structure determination of catalytic sites on Pd/Cu near surfaces alloys. *J. Phys. Chem. C* 113, 7246–7250 (2009).

23. Aaen, A. B., Lægsgaard, E., Ruban, A. V. & Stensgaard, I. Submonolayer growth of Pd on Cu(111) studied by scanning tunneling microscopy. *Surf. Sci.* 408, 43–56 (1998).

24. Tolman, R. C. The principle of microscopic reversibility. *Proc. Natl. Acad. Sci. U.S.A.* 11, 436–439 (1925).

25. Hager, T., Rauscher, H. & Behm, R. J. Interaction of CO with PdCu surface alloys supported on Ru(0001). *Surf. Sci.* 558, 181–194 (2004).

26. Illas, F. *et al.* Interaction of CO and NO with PdCu (111) Surfaces. *J. Phys. Chem. B* 102, 8017–8023 (1998).

27. Sakong, S., Mosch, C. & Groß, A. CO adsorption on Cu-Pd alloy surfaces: ligand versus ensemble effects. *Phys. Chem. Chem. Phys.* 9, 2216–2225 (2007).

28. Lopez, N. & Nørskov, J. K. Synergetic effects in CO adsorption on Cu-Pd(111) alloys. *Surf. Sci.* 477, 59–75 (2001).

29. Johnson, A. D., Daley, S. P., Utz, A. L. & Ceyer, S. T. The chemistry of bulk hydrogen: reaction of hydrogen embedded in nickel with adsorbed CH_3. *Science* 257, 223–225 (1990).

30. Stamatakis, M. & Vlachos, D. G. A graph-theoretical kinetic Monte Carlo framework for on-lattice chemical kinetics. *J. Chem. Phys.* 134, 214115–1–214115–13 (2011).

Author Contributions M.D.M., A.D.J., M.B.B., E.A.L., C.J.M., and G.K. performed the experiments. Data analysis was performed by M.D.M., A.D.J., G.K., and E.C.H.S. M.S. performed the KMC simulations and post-processing. The paper was written by M.D.M., G.K., M.S., and E.C.H.S.

Additional information Supplementary information is available in the online version of the paper. Reprints and permissions information is available online at www.nature.com/reprints. Correspondence and requests for materials should be addressed to E.C.H.S.

Competing financial interests The authors declare no competing financial interests.

Figure Legends:

Figure 1 | Preferred binding sites for Hydrogen and CO. (A) STM image of a Pd/Cu alloy with 1% Pd atoms in the surface Cu layer. The Pd/Cu alloy forms preferentially at the ascending step edge as evidenced by the rumpled appearance of the brim, whereas the lower terrace is composed of pure Cu. Scale bar = 10 nm. Inset shows atomic resolution of isolated Pd atoms in the Cu(111) surface. Scale bar = 1 nm **(B)** Adsorbed hydrogen atoms appear as depressions and cluster into islands on the Cu terraces. Scale bar = 4 nm. **(C)** Small amounts of deposited CO molecules appear as individual depressions and bind preferentially to the Pd sites in the alloy brim, which covers the upper right hand side of the STM image. Scale bar = 7 nm. **(D, E)** Same area before and after a single CO molecule (depression highlighted with blue circle) was removed with a 4.8 V pulse from STM tip. **(F)** Atomic resolution image of the same region after all the CO molecules were removed showing that individual Pd atoms (appearing as depressions with this STM tip state) are the preferred adsorption sites. Scale bar = 2 nm

Figure 2 | The molecular cork effect. Temperature programmed desorption spectra **A**: In the absence of CO, hydrogen desorption occurs from the 1% Pd/Cu surface at 210 K. Spectra **B**: Pre-dosing CO inhibits the uptake of hydrogen. Spectra **C**: Deposition of CO after hydrogen uptake leads to higher temperature (260 K) hydrogen desorption. The inset shows that the low temperature tail of the CO desorption trace extends down to 230 K at which point H_2 begins desorbing. Schematics **A-C** illustrate CO's effect on either blocking hydrogen uptake or trapping adsorbed hydrogen on the surface above its regular desorption temperature.
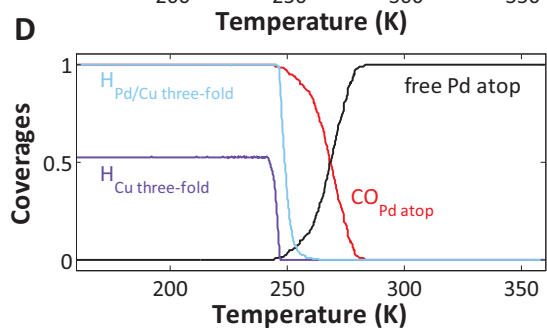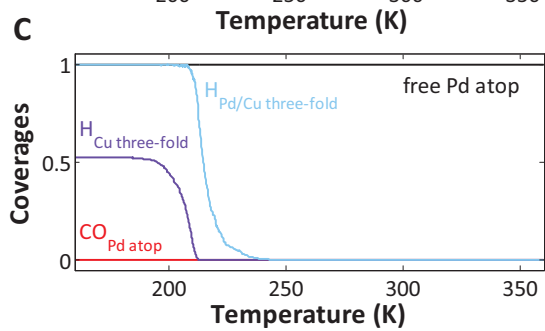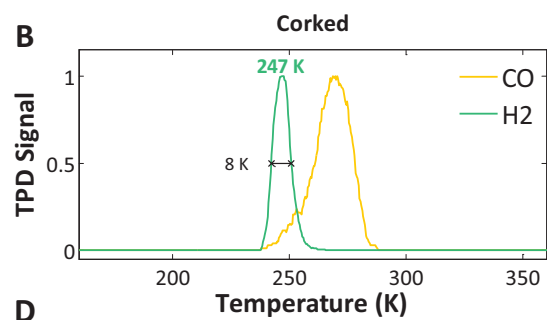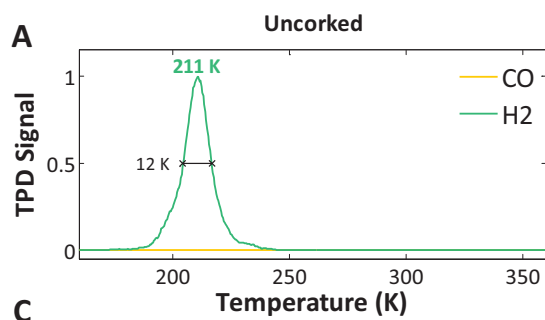
Figure 3 | Kinetic Monte Carlo simulations of the molecular cork effect. Temperature programmed desorption spectra for the uncorked **(A)** and the corked **(B)** systems capture both the peak position and shape changes observed experimentally. The H_a and CO coverage profiles for the uncorked **(C)** and the corked **(D)** system reveal that hydrogen coverage on the entrance/exit Pd/Cu sites remains high even when the coverage on the Cu sites has dropped significantly.
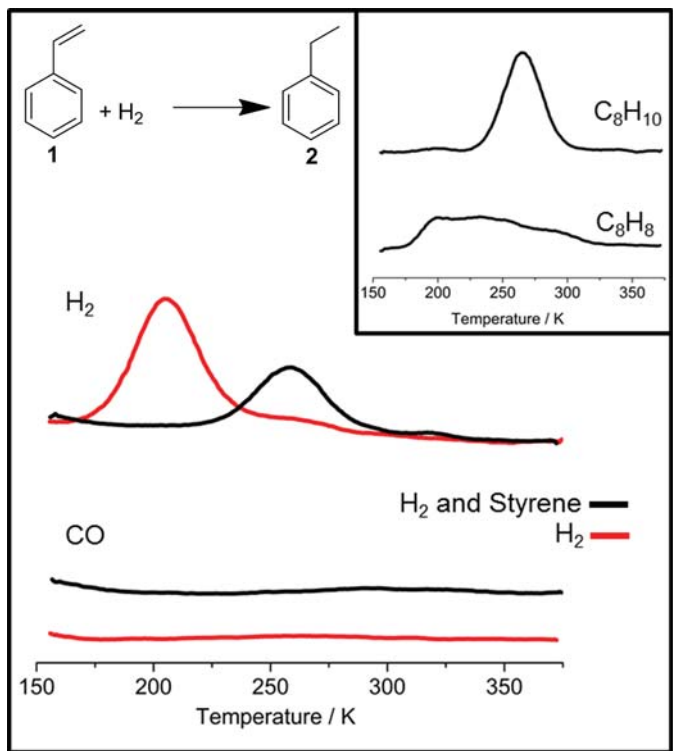
Figure 4 | The molecular cork effect in a hydrogenation reaction. Temperature programmed reaction spectra reveal that during the hydrogenation of styrene to ethylbenzene, surface hydrogen remains on the surface 55 K hotter than when no styrene is present. Desorption traces indicate that this cork effect occurs in the absence of CO, and therefore the reactants/products themselves act as a molecular cork trapping adsorbed hydrogen atoms on the surface in a higher energy state.

CO ——
H_2 ——

A

B

C

Temperature / K

Temperature (K)

Hydrogen Atom

Carbon Monoxide

H_2

H_2

A

H_2

H_2

B

C

A Uncorked

211 K

12 K

TPD Signal

- CO
- H2

Temperature (K)

B Corked

247 K

8 K

TPD Signal

- CO
- H2

Temperature (K)

C

Coverages

free Pd atop

$H_{Pd/Cu\ three-fold}$

$H_{Cu\ three-fold}$

$CO_{Pd\ atop}$

Temperature (K)

D

Coverages

$H_{Pd/Cu\ three-fold}$

free Pd atop

$H_{Cu\ three-fold}$

$CO_{Pd\ atop}$

Temperature (K)
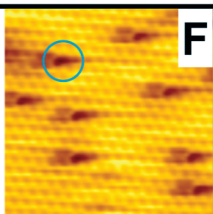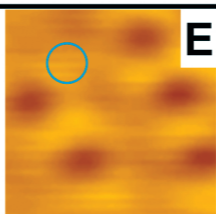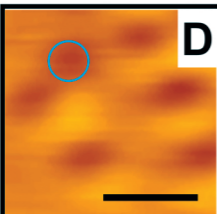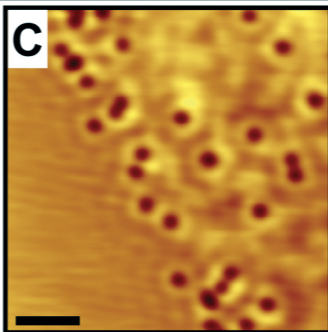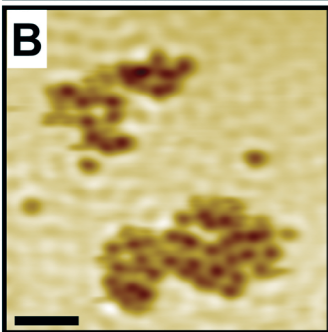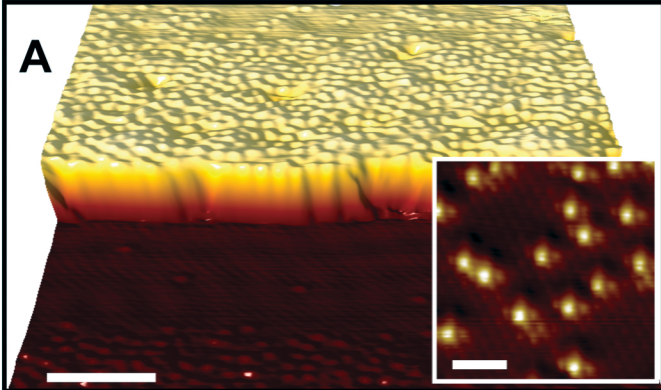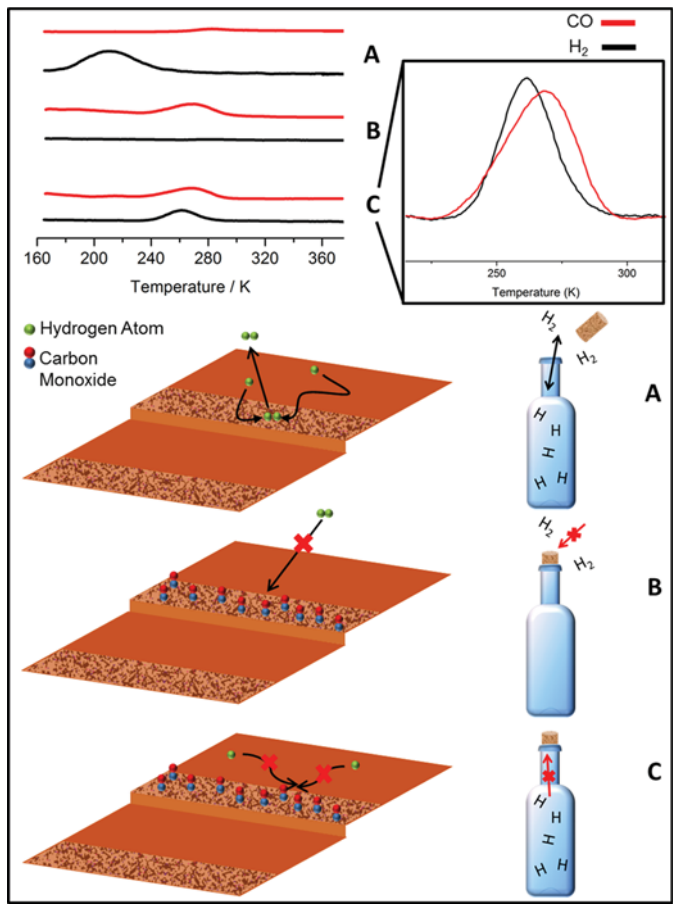
Controlling a Spillover Pathway with the Molecular Cork Effect

Matthew D. Marcinkowski, April D. Jewell, Michail Stamatakis, Matthew B. Boucher, Emily A. Lewis, Colin J. Murphy, Georgios Kyriakou & E. Charles H. Sykes

Molecular Manipulation to Probe CO Adsorption Sites on the Pd/Cu Alloy

To support our finding that CO preferentially occupies atomic Pd sites in the Cu/Pd surface alloy, we performed molecular manipulation experiments in which, using the STM tip, CO molecules were desorbed one-by-one[1] revealing the nature of the surface sites beneath with atomic resolution. Fig. S1 below shows an example in which individual CO molecules were removed one at a time from their preferred adsorption sites with a 4.8 V pulse before the same area was imaged with atomic resolution. These experiments reveal a perfect correlation between CO adsorption site and the individual Pd atoms in the surface beneath and show that one CO molecule is adsorbed above each Pd atom in the surface.
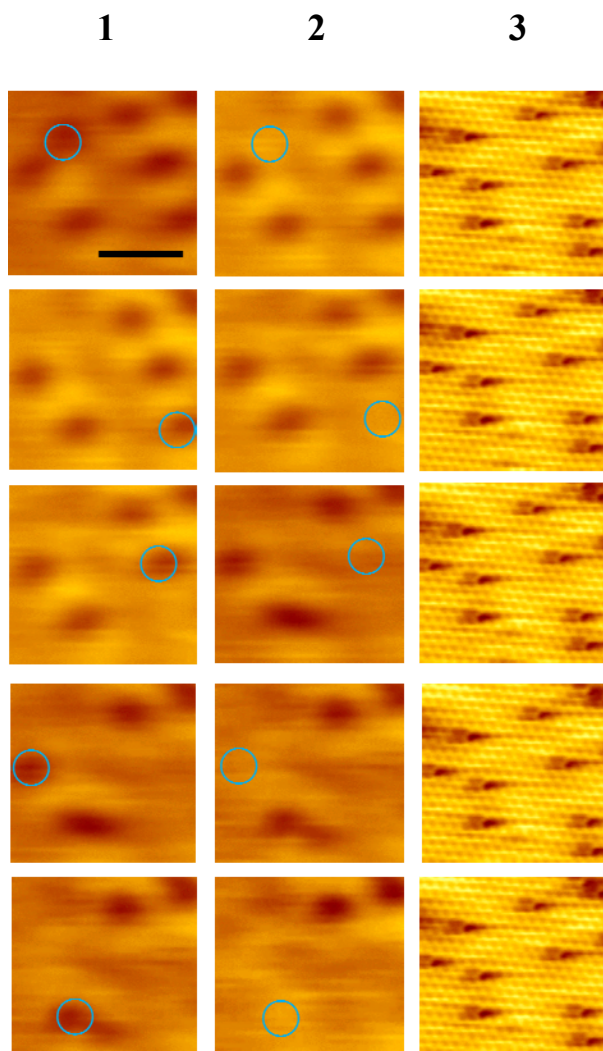
Supplementary Figure S1. High resolution STM imaging and manipulation of individual CO molecules (appearing as diffuse depressions) adsorbed at their preferred sites on the Pd/Cu alloy surface. The blue circles in column 1 highlight each point at which a 4.8 V pulse was used to remove a single CO molecule. Column 2 shows the same regions after each molecule was removed, and the atomic resolution images in column 3 were acquired after removal of all the CO molecules from the area and reveal an exact correlation between preferred adsorption site of each CO molecule and the Pd atoms (appearing as localized depressions) in the surface beneath. Scale bar = 2 nm.

Carbon monoxide on Cu(111)

CO adsorbs on Cu(111) without decomposition and saturates at an exposure of ≥ 8 L in our system in agreement with earlier reports[2]. The resulting TPD spectrum (Fig. S2) shows three distinct desorption peaks, which have previously been investigated in detail[2-4]. The low temperature peak (~110 K) is assigned to desorption from a densely packed (7 x 7) unit cell, the mid temperature peak (~ 130 K) to desorption of the intermediate (4 x 4) unit cell, and the largest peak, centred around 170 K to desorption from the $(\sqrt{3} \times \sqrt{3})$ unit cell. Saturation of CO on Cu(111) at low temperatures yields a (7 x 7) unit cell that corresponds to 0.52 ML, i.e. 0.52 CO molecules per surface Cu atom.
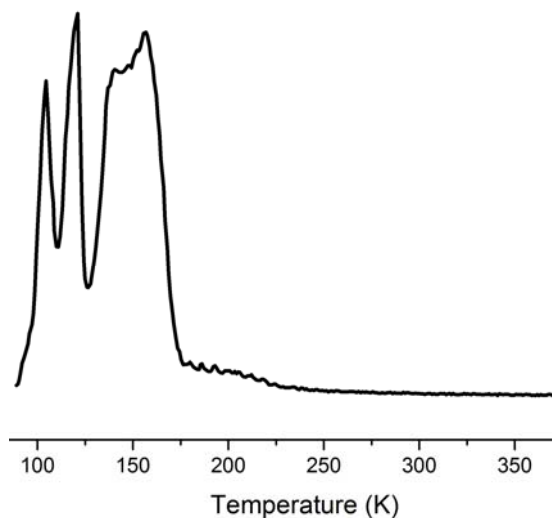
Supplementary Figure S2. CO TPD from clean Cu(111) after a saturation exposure of 10 L.

Carbon monoxide on 1% Pd in Cu(111)

Desorption of CO from a 0.01 ML Pd/Cu(111) SAA results in a TPD spectrum with very similar features to that of pure Cu(111) except for a small high temperature desorption peak of CO at 270 K which is correlated with CO binding at individual Pd atom sites as shown in the STM image in Fig. 1c-e in the manuscript. The TPD spectra in Fig. S3 show desorption of 10 L (black) and 0.1 L (red) CO from 0.01 ML Pd in Cu(111). The 10 L CO dose saturates the monolayer and looks almost identical to Fig. S2 except for the higher temperature peak associated with CO bound to Pd sites which indicates that in a 0.01 ML Pd/Cu(111) SAA the vast majority of the surface sites are Cu(111). The 0.1 L CO dose is enough to saturate the Pd sites and populate a small fraction of the available Cu surface as evidenced by the small peak at 160 K in the red trace.
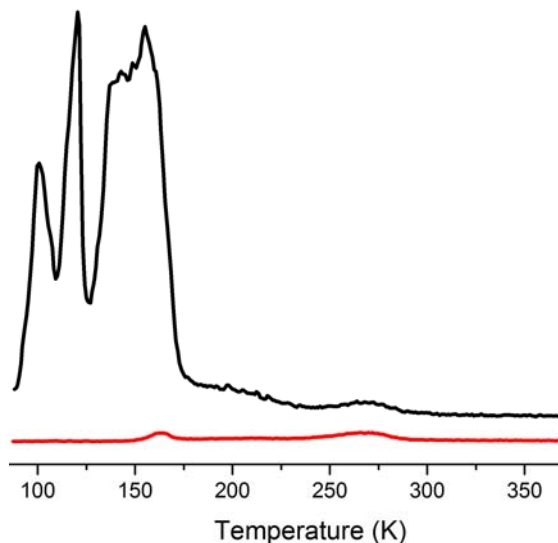
Supplementary Figure S3. CO TPD spectra from 0.01 ML of Pd in Cu(111) after a saturation CO exposure of 10 L (black) and 0.1 L (red).

Hydrogen Storage on Cu(111) via the Cork Effect

In order to investigate if the cork effect could be used to store hydrogen on the Cu(111) surface above its normal desorption temperature, we performed isothermal annealing experiments both with and without the CO cork. Hydrogen and CO were deposited at 85 K, the system was then ramped to the desired temperature, held for 10 min and then cooled to 150 K before the TPD spectra were acquired. This data, shown below in Fig. S4, reveals that when the system is uncorked, a 10 min anneal in a temperature window between 190 - 210 K leads to desorption of surface bound H. However, annealing the corked system under identical conditions results in retention of the surface-bound hydrogen. This provides direct evidence for storage of weakly bound H atoms that have spilled over onto Cu from Pd sites. Common hydrogen storage materials utilize small Pt/Pd particles to promote uptake by activating molecular H_2 and facilitating spillover of hydrogen atoms onto a support. Given that CO desorbs from low index Pd surfaces ~500 K we suggest that the molecular cork effect could be used to store hydrogen over a much wider range of temperatures in practical systems.
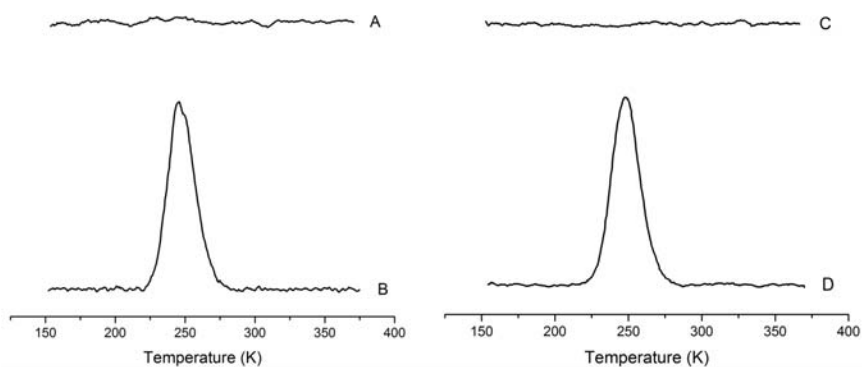

Supplementary Figure S4. TPD spectra for uncorked (A) and corked (B) hydrogen after a 190 K anneal for 10 min. TPD spectra for uncorked (C) and corked (D) hydrogen after a 210 K anneal for 10 min. These spectra indicate that in the uncorked system no hydrogen is left on the surface after annealing 190-210 K, however, with a CO cork the hydrogen is still present on the surface after an identical treatment.

Kinetic Monte Carlo (KMC) Methodology Details

For the KMC simulation the graph-theoretical KMC framework is used[5]. For the purposes of the simulation, one has to define a lattice structure, the binding configurations and corresponding energies, and a set of elementary events, i.e. adsorption, desorption and reaction steps.

Thus, the Pd/Cu catalytic surface is represented as a lattice in which the different types of atop (Pd and Cu) and three-fold (Cu, Pd/Cu) sites are taken explicitly into account as shown in Supplementary Fig. S5, and the number of sites as well as their effective surface area (entering the adsorption kinetic constant) are shown in Supplementary Table S1.
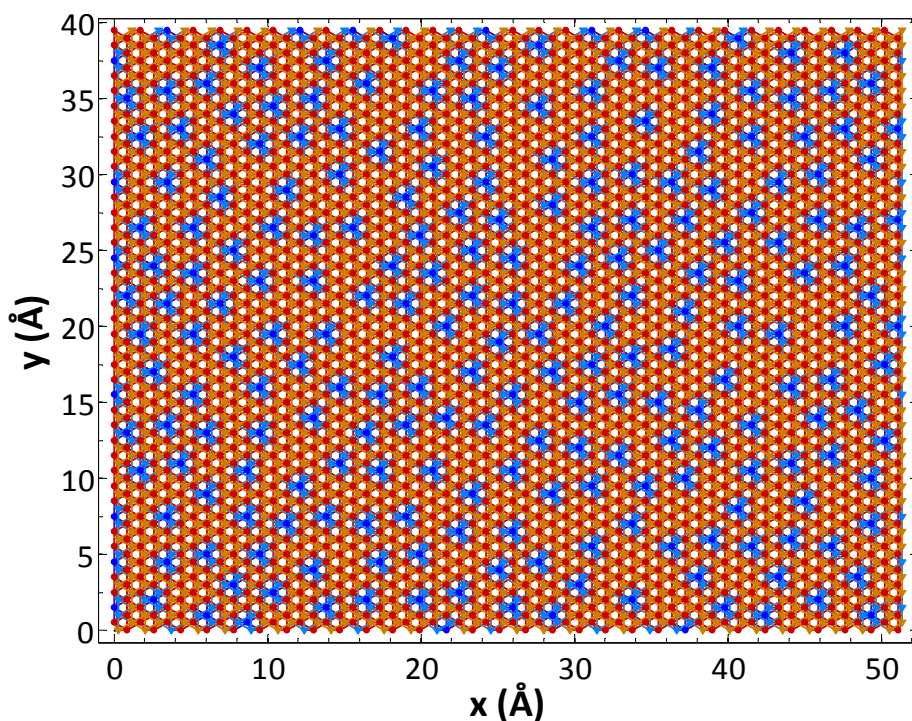
Supplementary Figure S5. Lattice structure representing the Cu/Pd surface. A legend is provided in Supplementary Table S1.
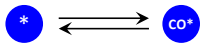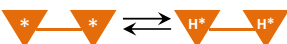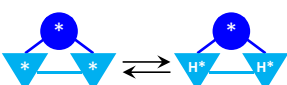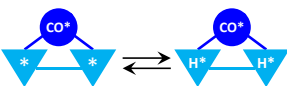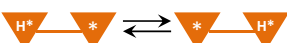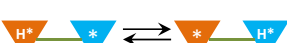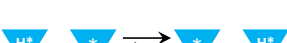
Supplementary Table S1. Site types and their properties.

Site Type	Symbol	Site Surface Area (Å^2)	Total Number of Lattice Sites
atop Cu	●	3.1	2163
three-fold Cu	▼	1.7	1689
atop Pd	●	4.2	237
three-fold Pd/Cu	▼	2.0	711

The simulation accounts for two binding configurations for H adatoms (on the three-fold Cu and three-fold Pd/Cu sites) and one for CO molecules (on the atop Pd sites). The binding energies are calculated with respect to CO and half a H_2 molecule in vacuum. The CO binding energy is taken as $BE_{Pd\ atop}^{CO} = 0.920$ eV, to capture the experimentally observed TPD peak around 270 K. The values of the H binding energies are taken from previous DFT calculations[6,7] and adjusted such that the simulated TPD peaks agree with the experimental ones, in particular, the values reported in the literature are: $BE_{Cu\ three-fold}^{H} = 0.14$ eV, and $BE_{Pd/Cu\ three-fold}^{H} = 0.24$ eV, and were adjusted to the following: $BE_{Cu\ three-fold}^{H} = 0.155$ eV, and $BE_{Pd/Cu\ three-fold}^{H} = 0.297$ eV.

Supplementary Table S2. Reactions and kinetic data.

Reaction Pattern	Description	A_{fwd} (s^{-1})	A_{fwd}/A_{rev}	E_a (eV)	ΔE_{rxn} (eV)
	CO adsorption	$1.314 \cdot 10^8$ bar^{-1}	$6.259 \cdot 10^{-9}$ bar^{-1}	0.000	−0.920
	H_2 dissociative adsorption on three-fold Cu	$9.221 \cdot 10^7$ bar^{-1}	$3.644 \cdot 10^{-7}$ bar^{-1}	0.662	−0.309
	H_2 dissociative adsorption on three-fold Pd/Cu in the absence of CO	$9.221 \cdot 10^7$ bar^{-1}	$3.644 \cdot 10^{-7}$ bar^{-1}	0.062	−0.593
	H_2 dissociative adsorption on three-fold Pd/Cu in the presence of CO	$9.221 \cdot 10^7$ bar^{-1}	$3.644 \cdot 10^{-7}$ bar^{-1}	1.062	−0.593
	H diffusion between three-fold Cu sites	$6.180 \cdot 10^{15}$	1.000	0.655	0.000
	H diffusion from three-fold Cu to Pd/Cu	$6.180 \cdot 10^{15}$	1.000	0.513	−0.142
	H diffusion between three-fold Pd/Cu sites	$6.180 \cdot 10^{15}$	1.000	0.655	0.000

With regard to the reaction scheme, there are seven elementary reactions that are taken into account as depicted in Supplementary Table S2. All steps are taken to be reversible, and the reaction energies (ΔE_{rxn}) are calculated from the binding energies of the products minus those of the reactants. The activation energies for the H_2 adsorption on three-fold Cu and Pd/Cu sites are taken from the literature[6] and adjusted to match the experimentally observed TPD peaks. In particular, the barrier for H_2 adsorption on Cu is reported to be ~0.5 eV; we have used a value of 0.662 eV which gives a TPD peak around 310 K in the KMC simulation. For H_2 adsorption on Pd/Cu, the barrier is reported ~0.02 eV; we use 0.062 eV, which gives a simulated TPD peak around 210 K. Further, for the dissociative adsorption of H_2 on three-fold Pd/Cu sites in the presence of CO, we set the barrier to a value 1 eV higher than that in the absence of CO to capture the corking effect. The pre-exponentials for the adsorption events have units of inverse pressure x time, and for the desorption, units of inverse time. For non-activated adsorption and the corresponding desorption (in the case of CO) the pre-exponentials are[5]:

$$A_{fwd}^{\substack{Non-Activated \\ Adsorption}} = \frac{p_X \cdot A_{st}}{\sqrt{2 \cdot \pi \cdot m_X \cdot k_B \cdot T}} \tag{1}$$

$$A_{rev}^{\substack{Non-Activated \\ Adsorption}} = \frac{q_{vib,X_{(gas)}} \cdot q_{rot,X_{(gas)}} \cdot q_{trans2D,X_{(gas)}}}{q_{vib,X}} \cdot \frac{k_B \cdot T}{h} \tag{2}$$

where, p_X is the pressure of the gas-phase species, A_{st} the effective site area (Supplementary Table S1), m_X the mass of the molecule, k_B the Boltzmann constant, and T the temperature. The $q_{vib,X_{(gas)}}$, $q_{rot,X_{(gas)}}$ and $q_{trans2D,X_{(gas)}}$ denote the vibrational, rotational and 2D translational quasi-partition functions of the gas-phase species, and $q_{vib,X}$ denotes the vibrational quasi-partition function of the adsorbed species, all of which are calculated using standard expressions[8]. For the activated adsorption:

$$A_{\text{fwd}}^{\overset{\text{Activated}}{\text{Adsorption}}} = \frac{q_{\text{vib}}^{\neq}}{q_{\text{vib},X_{(\text{gas})}} \cdot q_{\text{rot},X_{(\text{gas})}} \cdot q_{\text{trans2D},X_{(\text{gas})}}} \cdot \frac{p_X \cdot A_{\text{st}}}{\sqrt{2 \cdot \pi \cdot m_X \cdot k_B \cdot T}} \tag{3}$$

and for the desorption:

$$A_{\text{rev}}^{\overset{\text{Activated}}{\text{Adsorption}}} = \frac{q_{\text{vib}}^{\neq}}{q_{\text{vib},X}} \cdot \frac{k_B \cdot T}{h} \tag{4}$$

where $q_{\text{vib}}^{\neq}$ refers to the transition state. The data used in our calculations of the quasi-partition functions were found in the literature are shown in Supplementary Tables S3 and S4. All the pre-exponentials were calculated at $T = 250$ K.

Supplementary Table S3. Gas-phase species properties.

Species	Vibrational Frequency (cm^{-1})[9]	Moment of Inertia (eV/s^2)[10]	Symmetry Number[10]
CO	2134.81	$9.093 \cdot 10^{-28}$	1
H$_2$	4336.33	$2.946 \cdot 10^{-29}$	2

**Supplementary Table S4. Adsorbed species properties.**

Species	Vibrational Frequencies (cm^{-1})	Reference
CO$_{\text{Pd atop}}$	1894, 282, 188, 188, 108, 108	7
H$_{\text{Cu three-fold}}$	1013, 862, 862	7
TS for H$_2$ dissociation on Cu	1433, 1048, 807, 484, 403	11

The vibrational frequencies for H$_{\text{Pd/Cu three-fold}}$ were taken to be the same as H$_{\text{Cu three-fold}}$. The same applies to the vibrational frequencies for the transition state for H$_2$ dissociation on the three-fold Pd/Cu sites in the presence and absence of CO. Finally, diffusion events occur on a much faster time-scale than any other event. This disparity in the timescales hinders the efficient simulation of the system, since the algorithm spends most of the computational time executing diffusional hops rather than the more interesting desorption events. To overcome this issue (termed stiffness in KMC simulation) the barriers and pre-exponentials of the diffusion events were adjusted to reduce the number of diffusional hops per unit time, while ensuring that diffusion is still

sufficiently fast for the adlayer to remain equilibrated. The latter was tested by comparing the

coverages of $H_{Cu\ three-fold}$ and $H_{Pd/Cu\ three-fold}$. In quasi-equilibrium, these coverages follow Fermi-Dirac statistics:

$$\theta^{H}_{Cu\ three-fold} = \frac{1}{e^{\frac{-BE^{H}_{Cu\ three-fold} - \mu_{H}}{k_{B} \cdot T}} + 1} \qquad \text{and} \qquad \theta^{H}_{Pd/Cu\ three-fold} = \frac{1}{e^{\frac{-BE^{H}_{Pd/Cu\ three-fold} - \mu_{H}}{k_{B} \cdot T}} + 1} \qquad (5)$$

The chemical potential μ_{H} was determined by the total number of H adparticles that exist on the

lattice at a given time. Comparisons between the simulated coverages and those predicted by the

Fermi-Dirac statistics for single simulations of the uncorked and corked systems are shown

below in Fig. S6. The agreement between the two is excellent.
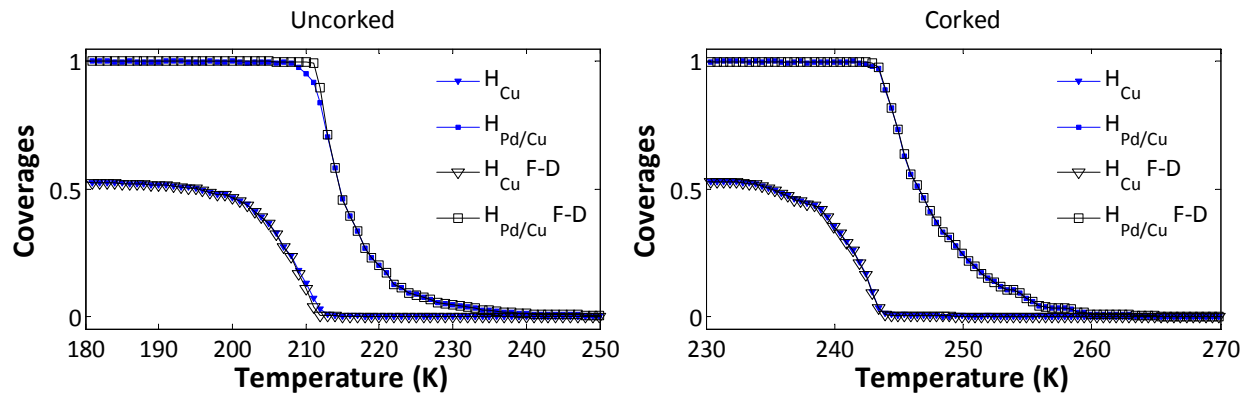
Supplementary Figure S6. Comparisons between the simulated surface coverages and those predicted by

**Fermi-Dirac statistics for the adsorbed hydrogen on the three-fold Cu and Pd/Cu sites.**

Statistics of Elementary Events
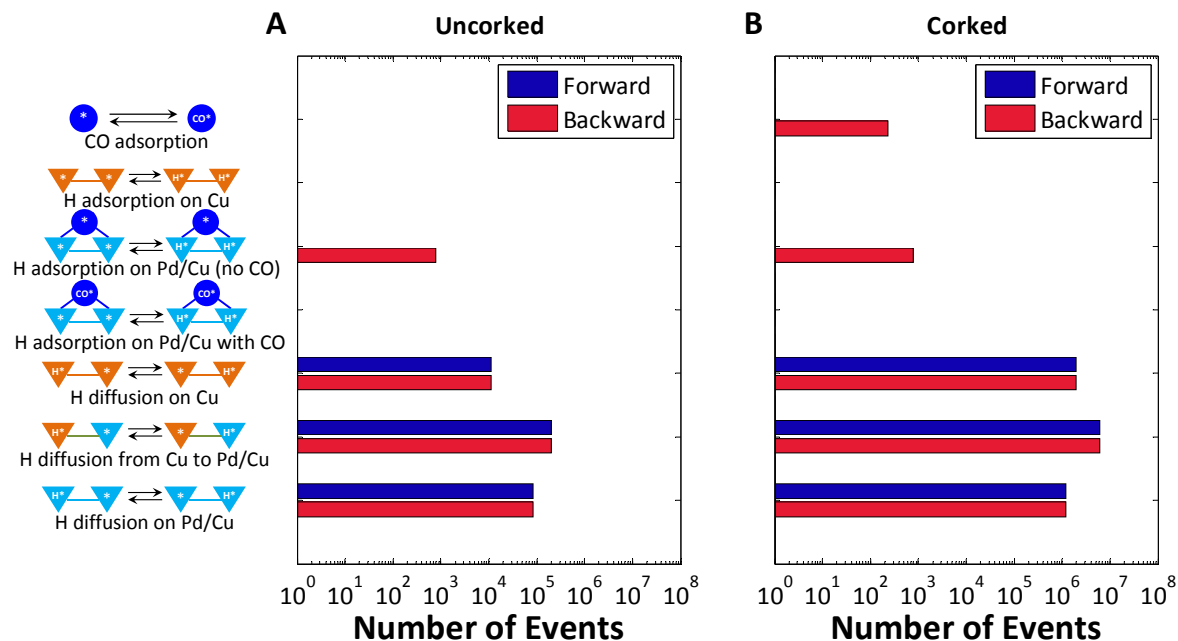
Supplementary Figure S7. Number of elementary reaction events executed throughout the course of a simulation for the uncorked and corked systems. For each reaction, the number of forward (blue bars) and backward (red bars) events are shown. The reactions are explained in Supplementary Table S2. In both cases H_2 desorption proceeds through the Pd/Cu sites in the absence of CO. Thus, in the corked system, H adatoms have to "wait" for CO to escape from at least one Pd atop site until they can associate and desorb. Moreover, the bar graphs show that diffusion is quasi-equilibrated (number of forward equal to number of reverse events), and occurs on a timescale much faster than desorption.

Hydrogenation of Styrene on 0.01 ML of Pd in Cu(111)

The presence of styrene on Cu(111) causes the surface hydrogen to be corked even at a coverage of 0.01 ML of styrene as evidenced by the hydrogen peak being shifted 55 K higher in temperature in the TPR spectrum Fig. S8 below. This TPR of styrene shows that effectively all styrene has converted to ethylbenzene at this low styrene coverage.
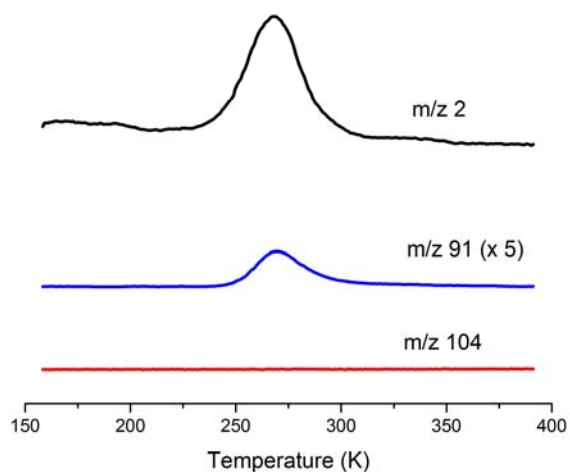
Supplementary Figure S8. TPR spectrum showing complete hydrogenation of styrene on a 0.01 ML of Pd in Cu(111) surface after a exposure to 200 L H_2 and 0.01 ML Styrene. M/z 2 corresponds to hydrogen, m/z 91 corresponds to ethylbenzene, and m/z 104 corresponds to styrene.

References

1. Bartels, L. *et al.* Dynamics of electron-induced manipulation of individual CO molecules on Cu(111). *Phys. Rev. Lett.* **80**, 2004–2007 (1998).

2. Raval, R., Parker, S., Pemble, M. & Hollins, P. FT-RAIRS, EELS and LEED studies of the adsorption of carbon monoxide on Cu(111). *Surf. Sci.* **203**, 353–377 (1988).

3. Kirstein, W., Krueger, B. & Thieme, F. CO adsorption studies on pure and Ni-covered Cu (111) surfaces. *Surf. Sci.* **176**, 505–529 (1986).

4. Kneitz, S., Gemeinhardt, J. & Steinrück, H. A molecular beam study of the adsorption dynamics of CO on Ru(0001), Cu(111) and a pseudomorphic Cu monolayer on Ru(0001). *Surf. Sci.* **440**, 307–320 (1999).

5. Stamatakis, M. & Vlachos, D. G. A graph-theoretical kinetic Monte Carlo framework for on-lattice chemical kinetics. *J. Chem. Phys.* **134**, 2141151–21411513 (2011).

6. Tierney, H. L., Baber, A. E., Kitchin, J. R. & Sykes, E. C. H. Hydrogen dissociation and spillover on individual isolated palladium atoms. *Phys. Rev. Lett.* **103**, 2461021–2461024 (2009).

7. Grabow, L. C. & Mavrikakis, M. Mechanism of methanol synthesis on Cu through CO_2 and CO hydrogenation. *ACS Catal.* **1**, 365–384 (2011).

8. McQuarrie, D. A. *Statistical Mechanics*. (Harper & Row, New York 2000).

9. Rohlf, J. W. *Modern Physics from α to Z^0* (John WIley, New York 1994).

10. Ott, J. B. & Boerio-Goates, J. *Chemical Thermodynamics: Advanced Applications*. (London Academic Press, London, 2000).

11. Hammer, B. & Scheffler, M. Multidimensional potential energy surface for H2 dissociation over Cu(111). *Phys. Rev. Lett.* **73**, 1400–1403 (1994).